Chemical and Materials Engineering Faculty Publications

Chemical and Materials Engineering

3-1-2017

Incorporating Poly(3-hexyl thiophene) into Orthogonally Aligned Cylindrical Nanopores of Titania for Optoelectronics

Suraj R. Nagpure
University of Kentucky, suraj.nagpure@uky.edu

James F. Browning
Oak Ridge National Laboratory

Stephen E. Rankin
University of Kentucky, stephen.rankin@uky.edu

Right click to open a feedback form in a new tab to let us know how this document benefits you.

Follow this and additional works at: https://uknowledge.uky.edu/cme_facpub

Part of the Chemical Engineering Commons, and the Materials Science and Engineering Commons

Incorporating Poly(3-hexyl thiophene) into Orthogonally Aligned Cylindrical Nanopores of Titania for Optoelectronics

Incorporating Poly(3-hexyl thiophene) into Orthogonally Aligned Cylindrical Nanopores of Titania for Optoelectronics

Suraj Nagpure[†], James F. Browning[‡], and Stephen E. Rankin[†,*]

[†] University of Kentucky, Chemical & Materials Engineering Department, 177 F.P. Anderson Tower, Lexington, KY 40506-0046 USA

[‡] Spallation Neutron Source, Oak Ridge National Laboratory, Oak Ridge, TN

* Author to whom correspondence should be addressed. E-mail: srankin@engr.uky.edu. Tel: +1-859-257-9799

Abstract

 The incorporation of hole conducting polymer poly(3-hexyl thiophene) (P3HT) into the 8-9 nm cylindrical nanopores of titania is investigated using films with a unique orthogonally oriented hexagonal close packed mesostructure. The films are synthesized using evaporation induced self-assembly (EISA) with Pluronic triblock copolymer F127 as the structure directing agent. The orthogonally oriented cylindrical nanopore structure was chosen over a cubic structure because confinement in uniform cylindrical channels is hypothesized to enhance hole conductivity of P3HT by inducing local polymer chain ordering. Orthogonal orientation of the cylindrical nanopores is achieved by modifying the substrate (FTO-coated glass slides) with crosslinked F127. After thermal treatment to remove organic templates from the films, P3HT is infiltrated into the nanopores by spin coating a 1 wt% P3HT solution in chlorobenzene onto the titania films followed by thermal annealing under vacuum at 200 °C. The results show that infiltration is essentially complete after 30 minutes of annealing, with little or no further infiltration thereafter. A final infiltration depth of ~14 nm is measured for P3HT into the nanopores of titania using neutron reflectometry measurements. Photoluminescence measurements demonstrate that charge transfer at the P3HT-TiO$_2$ interface improves as the P3HT is infiltrated into the pores, suggesting that an active organic-inorganic heterojuction is formed in the materials.

Keywords: titania, organic-inorganic, P3HT, oriented, nanopores

Introduction

Inorganic-organic hybrid bulk heterojunction solar cells have attracted considerable attention in recent years due to advantages such as low cost, tunable design, and simple fabrication processes that can be scaled for large-area devices [1-6]. In such bulk heterojunction solar cells, the active layer consists of an interdigitated or interpenetrating network of a conjugated polymer such as poly(3-hexylthiophene) (P3HT) as the donor material and an inorganic semiconductor (such as TiO_2, ZnO, CdS) as the electron acceptor. Out of all the inorganic-organic hybrid systems, TiO_2 is among the most widely used inorganic semiconductor in hybrid donor-acceptor blends because of advantages such as high availability, low toxicity and low cost. One major problem in hybrid solar cells, especially those composed of soft materials, is that the propensity for phase segregation leads to poor blending and morphological instability. This represents a significant hurdle to making good devices since enforcing acceptor and donor domain sizes on the order of a few nm is critical for good charge separation efficiency. One creative strategy to get around the phase segregation problem is to use templated inorganic hosts with nanoscale dimensions and backfill these with conjugated polymers. This approach has been used by many researchers using TiO_2-P3HT bulk heterojunctions with different morphologies of titania including nanotubes [7-12], nanoparticles [13], nanorods [13-19], pompons [8], and spherical nanoparticles [20]. All of these morphologies have dimensions of the range of 50-200 nm which is significantly higher than the diffusion length for P3HT (~5-20 nm [21-23]). Therefore there is a significant likelihood of recombination of electrons and holes generated in the P3HT before reaching the respective electrodes, which would be expected to lead to the poor efficiency. Thus, it is hypothesized that electron donor P3HT must be intermixed with titania that has features defined on the 10 nm length scale in order to obtain a high charge separation yield.

As a transparent and n-type semiconductor, TiO_2 is a promising metal oxide for photovoltaic and opto-electronic devices [24, 25] and has been used previously by many researchers to play different roles in photovoltaic devices such as antireflection coating [26, 27], the interlayer in organic solar cells [28], as electron transport material in dye-sensitized solar cells and hybrid solar cells [29-33]. However, little attention has been paid to the influence of the nanostructure of TiO_2 on the performance of heterojunction solar cells. McGehee and coworkers studied infiltration of P3HT into cubic nanopores of titania of approx. 10 nm diameter [23, 34, 35] and obtained a power conversion efficiency of 0.5 % after infiltration of P3HT into the nanopores of titania to a depth of 40 nm. They attributed the low effieciency to the polymer chain being able to coil within cubic nanopores rather than forming aligned chains where π-stacking would enhance charge carrier mobility. McGehee and coworkers have suggested that the hole conductivity of P3HT in the nanopores could be significantly enhanced if the chains were aligned by confinement by the surface of straight pore walls [35]. This was shown to be a promising direction for MEH-PPV, where titania films with 90 nm pores prepared by templating a 2D surface relief grating provided enhanced photocurrent compared to random particle arrays [36]. With this in mind, an ideal architecture for an inorganic-organic hybrid photovoltaic material is hypothesized to consist of P3HT infiltrated into vertically oriented cylindrical nanopores of titania with a pore diameter of ~10 nm.

The present work is the first to begin to address the infiltration of P3HT into vertically oriented cylindrical nanopores of titania with the long-term goal of increasing the efficiency of inorganic-organic hybrid photovoltaics based on these materials. The nanostructure employed here consists of continuous titania films with vertically aligned 2D hexagonal close packed (HCP) cylindrical nanopores with pore diameter of 8-9 nm. These films have a pore diameter

less than the diffusion length of P3HT, but two well-defined phases for conduction of charge carriers to each electrode [35]. In addition, the uniform cylindrical channels in these films are hypothesized to conduct holes 5 orders of magnitude faster than in interconnected cubic channels by confining polymer chains as regioregular, isolated wires rather than free coiled chains likely to be found cubic pores [34, 35]. Because of these features, films with orthogonally aligned HCP (o-HCP) channels are expected to be ideal components for improved solid state inorganic-organic hybrid photovoltaics.

The specific strategy employed to prepare the titania films uses evaporation induced self-assembly (EISA) [37] with Pluronic surfactant F127 as the structure-directing agent. F127 is a non-ionic triblock copolymer with molecular formula $EO_{106}PO_{70}EO_{106}$, where EO is ethylene oxide and PO is propylene oxide, and has average molecular weight of 12,500 Da. Titania films with o-HCP phase using Pluronic surfactant P123 (MW = 5800) have previously been synthesized [38-42]. The hypothesis behind using F127 to synthesize titania films is that since F127 has higher molecular weight than P123, it should produce larger pores than P123. Titania films with different morphologies and phases have been synthesized previously using F127 including cubic [43-50], hexagonal [47, 51-54], and nanowire microspheres [55]. The most important factor determining the final mesostructure is the molar ratio of F127 to titania precursor (M). According to Crepaldi et al. [47], titania films with hexagonal phase are obtained for M = 0.008 to 0.01 using titanium tetrachloride as titania precursor, ethanol as the solvent and F127 as the structure directing agent. A very well ordered hexagonal phase was found to be obtained for M = 0.01 [47] but because conventional oxide substrates were employed, the hexagonal films were oriented parallel to the solid surface. The new synthetic development reported here is the synthesis of o-HCP cylindrical nanopores using F127 and $TiCl_4$ by

5

modifying the glass substrate with cross-linked F127 prior to dip coating. The modifying layer is expected to be chemically "neutral" towards the F127 template, thus inducing the alignment of the HCP structure orthogonal to the film [38, 41]. The o-HCP oriented mesophase has been shown to form by a direct disorder-to-order transition for P123-templated TiO_2 films on glass slides modified with crosslinked P123 [41], and a similar mechanism is expected with F127. Very well ordered contrasting SEM images will be obtained for films cast onto plain glass and F127-modified glass indicating that glass modification works to provide vertical orientation of the nanopores. After confirming the o-HCP mesostructure, the infiltration of P3HT into the nanopores will be studied using UV-visible spectroscopy and neutron reflectometry, and the interactions between the two materials will be studied using photoluminescence measurements.

Experimental

NoChromix powder (Godax Laboratories, Inc.), sulfuric acid (95-98%, Sigma Aldrich), F127 (M_n ~ 12,500 Da, Sigma-Aldrich), 1,6-diisocyanatohexane (98%, Sigma Aldrich), glycerol (99+%, Sigma Aldrich), $TiCl_4$ (99.9%, Acros Organics), ethanol (200 Proof, Decon Laboratories), acetone (histological grade, Fisher Scientific), chlorobenzene (anhydrous 99.8%, Sigma-Aldrich), and regioregular P3HT (MW ~ 54,000-75,000 Da, Sigma-Aldrich) were all used as received.

Commercially available borosilicate glass slides were cleaned using NoChromix solution in concentrated sulfuric acid and modified based on the method of Koganti et al. [38] using F127 as the Pluronic surfactant. The solution was prepared by first adding 0.696 mmol/L of F127 and a drop of glycerol as a cross-linker to 100 ml acetone. An equal number of moles of 1,6-diisocyanatohexane was added dropwise to the mixture in a nitrogen-filled glove bag. The freshly prepared solution was then dip coated onto glass slides and the slides were aged at

120 °C overnight (approx. 12 hours) to drive the isocyanate-hydroxyl cross-linking reaction to completion. Titania films with F127 as the structure directing agent have been synthesized according to the procedure of Crepaldi et al. with a modified thermal treatment [47]. The coating solution was prepared by adding 0.01 mole (1.93 g) of $TiCl_4$ to a solution of 1.26 g F127 ($M = 0.01$) in 30 g anhydrous ethanol in a nitrogen-filled glove bag. To this solution, 0.1 mole (1.8 g) of water was slowly added and the sol was allowed to react for 10 minutes before coating. Films were prepared by dip coating glass substrates with the sol at room temperature. Titania films were aged after coating at a temperature of 4 °C for 2 hours at a relative humidity of approx. 94%. Titania films were then calcined by transferring them directly from the refrigerator to a muffle furnace and increasing the temperature at 25 °C/min to 400 °C and holding for 10 min followed by rapid cooling. Films were not only coated onto plain glass, but also onto modified glass in order to provide orthogonal alignment of cylindrical nanopores.

Vertically oriented mesoporous titania films were then used to study the infiltration mechanism of P3HT into the nanopores. 1 wt% P3HT solution was prepared in chlorobenzene with continuous stirring at 100 °C in a water bath to ensure complete dissolution. The P3HT solution (0.5 ml) was spin coated onto titania films using spin coater (Laurell Technologies Corporation, Model WS-400BZ-6NPP/LITE) at 1500 rpm for 45 seconds. In order to increase the infiltration of P3HT into pores, these films were then annealed at 200 °C in a vacuum oven at a pressure of 20 mm Hg for variable time. Annealing was done under vacuum because P3HT is sensitive to ambient air and can degrade in the presence of air or moisture.

For plan-view imaging of pore structures, scanning electron microscopy (SEM) was performed using a Hitachi S-4300 at 3 kV. SEM samples were prepared by cutting the glass slide to the desired shape using a glass cutter and then mounting them exactly at the center of SEM

stubs coated with carbon tape. The edges of the sample were coated with colloidal graphite (isopropanol base, Ted Pella, Inc.) to increase conductivity by keeping the top surface in electrical contact with the lower surface. The samples were aged at 120 °C overnight (approx. 12 hours) to evaporate all the solvent from the colloidal graphite solution. The GISAXS pattern of a representative titania film was collected at the Advanced Photon Source at Argonne National Labs on beamline 8-ID-E in order to confirm vertical orientation of the pores.

Infiltration of P3HT into the pores of titania was characterized using UV-visible spectroscopy with an Ocean Optics Jaz Spectrometer in transmission mode. Glass slides coated with thin films were positioned exactly vertically so that the spectrophotometer beam passed through glass slide and film in sequence. In order to quantify infiltration depth, neutron reflectometry experiments were performed at the Liquids Reflectometer (beamline 4B) at the Spallation Neutron Source (SNS) at Oak Ridge National Lab (ORNL). The reflectivity $R(Q)$, was measured as a function of perpendicular wave vector transfer, $Q = (4\pi/\lambda)\sin\theta$, where λ is the neutron wavelength and θ the angle between neutron beam and sample surface [56]. With the neutron spectrum covering wavelengths from 2.5 to 17.5 Å and three incident angles of $\theta = 0.30°$, $0.8°$, and $1.8°$, neutron reflectivity (NR) data were collected in time-of-flight mode. The films were prepared on 5 mm thick circular silicon wafers with a diameter of 50 mm by the same modification and dip coating procedures described above. All reflectivity measurements were performed at room temperature and atmospheric pressure. Photoluminescence (PL) spectra were measured using a Renishaw inVia Raman microscope (Model: RE02) operating at room temperature. The PL of P3HT infiltrated into nanoporous TiO_2 was measured at steady state by excitation using 442.1 nm light generated using a blue (HeCd) laser. The samples for PL were

stored under vacuum immediately after synthesis to avoid changes in PL behavior due to exposure to air, and analyzed within 24 hours of preparation.

Results and Discussion

Figure 1 shows representative SEM images of F127-templated films on plain glass and crosslinked F127-modified glass prepared with $M = 0.01$ and 30 g of ethanol. The thickness of the titania films was estimated using ellipsometry of films cast onto silicon wafers to be 120 nm. Prior studies have shown that the thickness of the films can be controlled at least within a range from 50 nm to 250 nm by changing the ethanol:Ti ratio [38], and a multilayer deposition technique is under development to expand the thickness of titania films with orthogonally oriented mesopores into the micron range. For films on plain glass (Fig. 1a), most of the time (approx. 8 out of 10 times that a region was sampled), parallel stripes were observed in SEM images, which is consistent with cylindrical pores primarily aligned parallel to the substrate. For films on modified glass, the contrast between titania wall and the empty pore is much better, and as Fig. 1b illustrates, very well ordered, accessible pores are observed, suggesting that orthogonal alignment of mesopores has been increased for films cast onto modified glass. However, these pores are not 100% orthogonally oriented and thus we also see parallel stripes in some SEM images for the film on modified glass with $M = 0.01$. However, the frequency of parallel stripes was less than for unmodified glass, having been observed 3 out of 10 times. These SEM images suggest that a 2D HCP microstructure is formed with a pore diameter of about 8-9 nm for orthogonal pores. The unit cell parameter, which here corresponds to the distance between the center of consecutive pores, is 14.5 nm. Selected area electron diffraction and high resolution transmission electron microscopy (Supporting Information Figure S1) were

applied to the materials and showed that the walls of the material are a mixture of amorphous TiO$_2$ with small anatase crystallites.

Figure 2a shows the GISAXS pattern of a TiO$_2$ film on modified glass after calcination at 400° C and Fig. 2b the corresponding 1D linecut derived by integrating along the q$_z$ direction within the upper part of the strongest Bragg rod from 0.08-0.1 Å^{-1}. The GISAXS pattern clearly shows two intense vertical rods located on both sides of the beam stop, q$_y$ = ±0.042 Å^{-1} indexed to the (100) plane of the HCP structure. The d-spacing calculated from the GISAXS pattern is 15 nm. Also from the linecut (figure 2b), we can see a diffraction peak of low intensity approximately at q$_y$ = 0.083Å^{-1}, with a d-spacing of 7.55 nm, indexed to the (200) plane of the HCP structure. There is another pair of in-plane diffraction spots within the Yoneda band at q$_y$ = ±0.05 Å^{-1} which is speculated to be caused by a layer of the o-HCP material which has undergone contraction. No distinct out of plane diffraction spots are visible. The presence of the vertical rods and absence of out of the plane diffraction spots clearly indicate that orthogonally oriented HCP pores are indeed present for the titania film prepared on modified glass. Cross sectional SEM of a fractured film (Supporting Information Figure S2) provided final confirmation of the o-HCP structure.

Our initial hypothesis was that F127 should produce pores of larger diameter than those obtained using P123, as it has higher molecular weight than P123. However, when measured, the pore diameter for these mesoporous films was the same as obtained using P123 (8-9 nm) [40]. The difference between F127 and P123 is that F127 (EO$_{106}$PO$_{70}$EO$_{106}$) has longer hydrophilic PEO (polyethylene oxide) blocks than P123 (EO$_{20}$PO$_{70}$EO$_{20}$). The likely reason that longer PEO blocks of F127 do not expand the pore size is that PPO (polypropylene oxide) blocks dictate the pore size while PEO mixes with titania matrix. The (100) diffraction peak for

P123 templated titania films is observed at $q_y = 0.048$ Å^{-1} [40] corresponding to a d-spacing of 13 nm. The d-spacing using F127 (15 nm) is slightly larger, indicating that mixing of PEO blocks with TiO$_2$ precursor leads to thicker walls when F127 is used as the template. Similar results were reported by Feng et al. who reported a 2.4 nm increase in wall thickness for F127-tempalted silica films compared to P123-templated films, while the pore size remained the same [57]. Although F127 did not produce larger diameter pores than films made using P123, the characterization results demonstrate that the synthetic strategy reported by Koganti et al. [38] can be generalized to generate o-HCP titania films using other Pluronic surfactants. The thicker walls may impart stability to the films for further processing, although this advantage is not within the scope of the current study.

After titania films with o-HCP nanopores were successfully synthesized using F127, the pores were infiltrated with the hole conducting polymer P3HT in order to begin the process of creating a bulk heterojunction for hybrid solar cells. To do this, the o-HCP films were spin coated using a 1 wt.% P3HT solution in chlorobenzene followed by annealing at 20 mm Hg and 200 °C for variable time periods. To rule out the posibility of P3HT undergoing degradation during annealing because of oxidation of alkyl side chains or the thiophene ring (which disrupts the π-conjugation and reduces the intensity of the absorption band accompanied with a blue shift [58]), a control experiment was performed with regioregular P3HT cast onto cleaned plain glass followed by annealing under the same conditions as the P3HT on o-HCP titania films. Figure 3a shows UV-vis absorption spectra of regioregular P3HT during annealing at 200 °C for times from 15 min to 5 hour. No changes in the absorption spectra of regioregular P3HT are observed with increasing annealing time, indicating that the polymer remains stable at this temperature and pressure. The absorption spectrum of P3HT features a maximum at ~520 nm which is attributed

to the electron transition from the valence band (HOMO) to the conduction band (LUMO) of P3HT. The absorption spectrum also features two shoulder peaks at 550 nm and 600 nm, which are attributed to inter-chain absorption coming from locally ordered domains, i.e., interstrand π-conjugation [59]. The presence of absorption peaks of the same intensity with no blue shift throughout the annealing time demonstrates no change in chain structure or interactions simply due to annealing and cooling back to room temperature.

Figure 3b shows UV-vis absorption spectra of P3HT infiltrated into o-HCP titania films at 200 °C. The spectra of infiltrated P3HT are compared with the absorption spectrum of regioregular P3HT on glass in Fig. 3b. According to Brown et al. [59], when P3HT is infiltrated into the nanopores of titania, a blue shift relative to regioregular P3HT is observed, due to reduced π-π stacking of polymers confined within the pore. This blue shift with respect to regioregular P3HT is consistent with infiltration of P3HT into the pores of titania and is taken as preliminary evidence that infiltration is occurring. The as-spun P3HT on a mesoporous titania film displays little or no blue shift with respect to regioregular P3HT, as expected prior to incorporation. As the annealing time increases, the P3HT absorbance band displays a monotonic blue shift consistent with gradual infiltration into the titania pores. The magnitude of this blue shift increases with annealing time up to a plateau of about 7-8 nm after 60 min of annealing, consistent with previous reports of P3HT infiltration [23, 60].

A plot of blue shift of the maximum absorbance as a function of annealing time (Figure 4a) indicates a rapid increase during the first 30 min, followed by a plateau from 60 min on. Along with the blue shift, the intensity of the shoulder peak at 600 nm due to interstrand π-conjugation decreases during infiltration. The most likely reason for change is that the infiltration reduces the degree of inter-chain order in the microcrystalline domains of P3HT, as

P3HT is confined into the nanopores of titania. According to Kim et al. [60], this reduction in intensity of the shoulder peak at 600 nm is consistent with the infiltration of the polymer. However, the shoulder peak does not vanish completely, which suggests that all the P3HT might not have been infiltrated into the porous titania film. P3HT which has not been infiltrated might have formed an overlayer at the top surface that gives rise to the shoulder peak after infiltration.

The rate of P3HT infiltration was also studied by measuring optical density of the infiltrated polymer after removing unincorporated polymer from the top of the film by ultrasonicating the films in toluene for 20 minutes (Figure 4b). The optical density increases with time from a small background value with no annealing, up to a plateau of ~0.2 from 60 min of annealing onwards. However, it is unreliable to estimate infiltration depending upon the optical density of the embedded polymer since it is possible that the P3HT overlayer might not have been rinsed off completely. Thus, we need a different technique to directly determine the infiltration depth of the polymer.

In order to quantify the infiltration depth, neutron reflectometry was performed. Reflectivity (R) data were obtained as a function of the wave vector transfer, Q for films with varying times of annealing and the data were analyzed using Motofit [61] software as implemented in Igor Pro. After analyzing the data, the model was fitted to the R vs. Q resulting in a multilayer neutron scattering length density (NSLD) profile as a function of normalized film depth. A materials' SLD relates its chemical composition and density according to the relationship as follows:

$$\text{NSLD} = \frac{N_a \rho_m}{M} \sum_{i=1}^{n} b_i \tag{1}$$

where M is molecular weight of the compound, N_a is Avogadro's number, ρ_m mass density and b_i the bound coherent scattering length of ith atom comprising the material [56]. These are calculated using the SLD calculator in Motofit. The theoretically calculated NSLD for nonporous titania is 2.34×10^{-6} $Å^{-2}$ based on the mass density of 3.78 g/cm^3 for anatase titania. From the top view SEM image, the porosity calculated for titania films with vertically oriented cylindrical nanopores is 45-47% (based on pore diameter of 8-9 nm and unit cell parameter of 14.5 nm), which would give a NSLD of 1.24×10^{-6} $Å^{-2}$. The theoretically calculated NSLD for P3HT is 0.68×10^{-6} $Å^{-2}$ based on the mass density of 1.1 g/cm^3 for bulk P3HT. Previously, Rawolle et al. studied the infiltration of polymer hole-conductor into mesoporous titania and reported the NSLD of 0.705×10^{-6} $Å^{-2}$ for a compact P3HT layer and NSLD of 1.67×10^{-6} $Å^{-2}$ for P3HT infiltrated into the nanopores of titania with 41% porosity [62]. Considering the porosity of the mesoporous films and NSLD of each material, the NSLD of P3HT infiltrated into the nanopores of titania is expected to be a volume-weight average value of 1.6-1.7×10^{-6} $Å^{-2}$.

Figure 5 shows the neutron reflectivity profile of P3HT infiltrated into the nanopores of titania after annealing at 200° C for 30 minutes, with a NSLD profile in the inset. The model matches very well with the experimental data. The NSLD profile that fits the data has four distinct layers: a bottom silica substrate, a nanoporous titania layer near the substrate, an interfacial P3HT layer infiltrated into the nanopores, and a top uniform P3HT layer. Attempting to fit the data with only three layers led to a significantly worse fit. The NSLD values of different layers obtained after fitting match very well with the theoretically calculated NSLD values. The best-fit parameters including the thickness, NSLD and surface roughness of each layer are summarized in Table 1 for 30 min of annealing. The profile clearly indicates the infiltration of P3HT about 14 nm into the nanopores of titania. Thus, the blue shift obtained in UV-Vis

spectroscopy studies was indeed because of the infiltration of the polymer and neutron reflectivity confirms the infiltration.

Figure 6 shows the neutron reflectivity profile of P3HT infiltrated into the nanopores of titania after annealing at 200° C for 60 min. The fitting results are similar to those for Figure 6, and there is not much change in the infiltration depth of the polymer after increasing annealing time. Even after 2 hours of annealing, an infiltration depth of 14 nm is still observed (data not shown but similar to Fig. 6). Thus, the plateau in blue shift and shoulder intensity decrease in Fig. 4 were, as expected, a result of having reached a maximum level of infiltration of the polymer into the pores. The infiltraton depth is lower than that obtained in previous studies [23, 34], which reported a maximum infiltration depth of 40 nm or more for cubic mesoporous titania. However, a monotonic decrease in the external quantum efficiency was reported in those studies as the infiltration depth increased, which indicates that charge generation mostly occurs near the top of the TiO_2 film [34, 35]. Thus, the holes generated below 10-20 nm below the top of TiO_2 film might undergo recombination with the electron from TiO_2 before escaping the P3HT-TiO_2 region since polymer chains located in the bottom of TiO_2 might act as the filter layer which prevents light from reaching the top of the interface [63]. Therefore, an infiltration depth of 14 nm may be sufficient for efficient solar cell performance. The reason for higher infiltration of P3HT within the first 30 minutes might be that the solvent chlorobenzene that we used to make the P3HT solution evaporated with increasing annealing time. The rate of evaporation of chlorobenzene is likely to be higher than the rate of infiltration of the polymer. After the one hour of annealing time, all the chlorobenzene should have evaporated. After this time, the infiltrated, solidified P3HT blocked the pores as a result of which, there is no further infiltration of P3HT with increasing annealing time. Another related reason for the reduced infiltration of P3HT into

15

cylindrical channels is entropic; in order to enter into the pores, the chains are forced to adopt an elongated configuration less entropically favorable than the coiled configuration found in solution and in free melts. Polymers confined within anodized alumina membrane pores have been shown to form a layer of reduced mobility near the pore wall, and alteration in crystallinity has been observed under extreme confinement [64]. These effects would be expected to inhibit the transport of neat P3HT into the pores. The shallow depth of penetration suggests that there may be an opportunity in the future to optimize photovoltaic performance by decreasing the TiO_2 layer thickness to minimize the electron transport distance.

The efficiency of electron transfer at the interface between P3HT and nanoporous TiO_2 can be investigated indirectly by means of photoluminescence (PL) quenching (Figure 7) [7, 65]. The PL spectrum of regioregular P3HT shows a characteristic emission pattern with two peaks in the 550-740 nm wavelength range [66]. The PL emission peak at around 600 nm can be assigned to the pure electronic transition and the peak at around 700 nm is assigned to the first vibronic band [67]. While the spectra exhibit significant noise because the films are so thin, the intensity of the PL spectrum decreases considerably as the P3HT-TiO_2 interface develops. The decrease in intensity or the quenching of both the peaks indicates efficient energy or charge transfer across the P3HT-TiO_2 interface. In other words, the quenching indicates reduced recombination within P3HT as the charge is transferred to TiO_2 and efficient exciton dissociation, as shown in other studies [68-71]. As observed for the other measurements above, the PL intensity decreases most rapidly during the first 30 min of annealing, followed by a plateau in quenching (Fig. 7b). This is also consistent with the UV-Vis spectroscopy data indicating that infiltration occurs over the first 30 minutes of annealing and plateaus thereafter. Thus, infiltration correlates with the charge transfer at the interface, which suggests that an active p/n heterojunction is present in these

systems which can be developed in future studies to understand photovoltaic performance and the effect of polymer confinement on organic-inorganic hybrid solar cells. Even though the infiltration depth is smaller than the previous reports [23, 34, 35], the infiltration depth is consistent with the active layer reported previously and the nanowire architecture of the incorporated polymer is expected to provide higher hole mobility of P3HT chains in the nanopores, which would improve the performance of P3HT-TiO$_2$ hybrid solar cells.

Conclusions

We have synthesized titania thin films with vertically oriented 2D-HCP cylindrical nanopores using Pluronic triblock copolymer surfactant F127. The pore size of F127 templated titania films is the same as that of P123-templated titania films because both surfactants have the same content of hydrophobic block (PPO) and but F127 provides a higher wall thickness because of its larger hydrophilic block (PEO). Regioregular P3HT has been incorporated into the vertically oriented cylindrical nanopores of the resulting films. An infiltration depth of ~14 nm is obtained after 30 minutes of annealing at 200 °C under vacuum and for higher annealing times, there is no further improvement in the infiltration depth. This infiltration is measured directly by neutron reflectivity, and causes a corresponding blue shift in the absorbance of the P3HT. The infiltration depth is lower than that reported in previous studies, most likely because of the higher cost of confinement of P3HT chains into straight cylindrical nanopores. The charge transfer across the P3HT-TiO$_2$ interface is significant and correlates with the degree of infiltration of P3HT. In the future, these results can be used to fabricate efficient solar cells by using the knowledge gained about the optimal conditions for incorporation of P3HT into the pores of orthogonal HCP titania films and comparing the performance with cubic nanopore arrangement of titania and planar titania.

Acknowledgments

References

[1] N. Lu, S. Chen, H. Wang, X. Quan, H. Zhao, Synthesis of molecular imprinted polymer modified TiO_2 nanotube array electrode and their photoelectrocatalytic activity, J. Solid State Chem., 181 (2008) 2852-2858.

[2] S. Tepavcevic, S.B. Darling, N.M. Dimitrijevic, T. Rajh, S.J. Sibener, Improved Hybrid Solar Cells via in situ UV Polymerization, Small, 5 (2009) 1776-1783.

[3] K.J. Jiang, K. Manseki, Y.H. Yu, N. Masaki, K. Suzuki, Y.L. Song, S. Yanagida, Photovoltaics Based on Hybridization of Effective Dye-Sensitized Titanium Oxide and Hole-Conductive Polymer P3HT, Adv. Funct. Mater., 19 (2009) 2481-2485.

[4] B. Muktha, D. Mahanta, S. Patil, G. Madras, Synthesis and photocatalytic activity of poly(3-hexylthiophene)/TiO_2 composites, J. Solid State Chem., 180 (2007) 2986-2989.

[5] M. Mall, P. Kumar, S. Chand, L. Kumar, Influence of ZnS quantum dots on optical and photovoltaic properties of poly(3-hexylthiophene), Chem. Phys. Lett., 495 (2010) 236-240.

[6] R. Po, M. Maggini, N. Camaioni, Polymer Solar Cells: Recent Approaches and Achievements, J. Phys. Chem. C, 114 (2009) 695-706.

[7] Y. Li, C.W. Wang, Y. Zhao, J. Wang, F. Zhou, Performance improvement of P3HT/TiO_2 coaxial heterojunction polymer solar cells by introducing a CdS interface modifier, J. Solid State Chem. , 196 (2012) 349-355.

[8] T.H. Zhang, L.Y. Piao, S.L. Zhao, Z. Xu, Q. Wu, C. Kong, Application of TiO_2 with different structures in solar cells, Chin. Phys. B, 21 (2012) 118401.

[9] Y. Hao, Y. Cao, B. Sun, Y. Li, Y. Zhang, D. Xu, A novel semiconductor-sensitized solar cell based on P3HT@CdS@TiO_2 core-shell nanotube array, Sol. Ener. Mater. Sol. Cells, 101 (2012) 107-113.

[10] J. Lee, J.Y. Jho, Fabrication of highly ordered and vertically oriented TiO_2 nanotube arrays for ordered heterojunction polymer/inorganic hybrid solar cell, Sol. Ener. Mater. Sol. Cells, 95 (2011) 3152-3156.

[11] S. Yodyingyong, X. Zhou, Q. Zhang, D. Triampo, J. Xi, K. Park, B. Limketkai, G. Cao, Enhanced Photovoltaic Performance of Nanostructured Hybrid Solar Cell Using Highly Oriented TiO_2 Nanotubes, J. Phys. Chem. C, 114 (2010) 21851-21855.

[12] K. Sanghoon, G.K. Mor, M. Paulose, O.K. Varghese, K. Shankar, C.A. Grimes, Broad Spectrum Light Harvesting in TiO_2 Nanotube Array - Hemicyanine Dye - P3HT Hybrid Solid-State Solar Cells, IEEE J. Sel. Top. Quantum Electr., 16 (2010) 1573-1580.

[13] C.C. Lin, P.H. Ho, C.L. Huang, C.H. Du, C.C. Yu, H.L. Chen, Y.C. Yeh, S.S. Li, C.K. Lee, C.W. Pao, C.P. Chang, M.W. Chu, C.W. Chen, Dependence of Nanocrystal Dimensionality on the Polymer Nanomorphology, Anisotropic Optical Absorption, and Carrier Transport in P3HT:TiO_2 Bulk Heterojunctions, J. Phys. Chem. C, 116 (2012) 25081-25088.

[14] Y. Lin, Q. Wei, G. Qian, L. Yao, J. Watkins, Morphology Control in TiO_2 Nanorod/Polythiophene Composites for Bulk Heterojunction Solar Cells Using Hydrogen Bonding, Macromolecules, 45 (2012) 8665-8673.

[15] J. Wang, T. Zhang, D. Wang, R. Pan, Q. Wang, H. Xia, Influence of CdSe quantum dot interlayer on the performance of polymer/TiO$_2$ nanorod arrays hybrid solar cell, Chem. Phys. Lett., 541 (2012) 105-109.

[16] T. Xu, M. Yan, J.D. Hoefelmeyer, Q. Qiao, Exciton migration and charge transfer in chemically linked P3HT-TiO$_2$ nanorod composite, RSC Adv., 2 (2012) 854-862.

[17] T.W. Zeng, C.C. Ho, Y.C. Tu, G.Y. Tu, L.Y. Wang, W.F. Su, Correlating Interface Heterostructure, Charge Recombination, and Device Efficiency of Poly(3-hexyl thiophene)/TiO$_2$ Nanorod Solar Cell, Langmuir, 27 (2011) 15255-15260.

[18] Y.C. Huang, J.H. Hsu, Y.C. Liao, W.C. Yen, S.S. Li, S.T. Lin, C.W. Chen, W.F. Su, Employing an amphiphilic interfacial modifier to enhance the performance of a poly(3-hexyl thiophene)/TiO$_2$ hybrid solar cell, J. Mater. Chem., 21 (2011) 4450-4456.

[19] J. Bouclé, S. Chyla, M.S.P. Shaffer, J.R. Durrant, D.D.C. Bradley, J. Nelson, Hybrid Solar Cells from a Blend of Poly(3-hexylthiophene) and Ligand-Capped TiO$_2$ Nanorods, Adv. Funct. Mater., 18 (2008) 622-633.

[20] W. Guo, Y. Shen, M. Wu, T. Ma, Highly efficient inorganic-organic heterojunction solar cells based on SnS-sensitized spherical TiO$_2$ electrodes, Chem. Commun., 48 (2012) 6133-6135.

[21] J.M. Nunzi, Organic photovoltaic materials and devices, C. R. Phys., 3 (2002) 523-542.

[22] J.E. Kroeze, T.J. Savenije, M.J.W. Vermeulen, J.M. Warman, Contactless Determination of the Photoconductivity Action Spectrum, Exciton Diffusion Length, and Charge Separation Efficiency in Polythiophene-Sensitized TiO$_2$ Bilayers, J. Phys. Chem. B, 107 (2003) 7696-7705.

[23] K.M. Coakley, Y. Liu, M.D. McGehee, K.L. Frindell, G.D. Stucky, Infiltrating Semiconducting Polymers into Self-Assembled Mesoporous Titania Films for Photovoltaic Applications, Adv. Funct. Mater., 13 (2003) 301-306.

[24] L. Forro, O. Chauvet, D. Emin, L. Zuppiroli, H. Berger, F. Lévy, High mobility n-type charge carriers in large single crystals of anatase (TiO$_2$), J. Appl. Phys., 75 (1994) 633-635.

[25] F. Campus, P. Bonhôte, M. Grätzel, S. Heinen, L. Walder, Electrochromic devices based on surface-modified nanocrystalline TiO$_2$ thin-film electrodes, Sol. Ener. Mater. Sol. Cells, 56 (1999) 281-297.

[26] K. Nakayama, T. Kubo, Y. Nishikitani, Electrophoretically Deposited TiO$_2$ Nanotube Light-Scattering Layers of Dye-Sensitized Solar Cells, Jpn. J. Appl. Phys., 47 (2008) 6610-6614.

[27] T. Fujibayashi, T. Matsui, M. Kondo, Improvement in quantum efficiency of thin film Si solar cells due to the suppression of optical reflectance at transparent conducting oxide/Si interface by TiO$_2$/ZnO antireflection coating, Appl. Phys. Lett., 88 (2006) 183508.

[28] R. Steim, F.R. Kogler, C.J. Brabec, Interface materials for organic solar cells, J. Mater. Chem., 20 (2010) 2499-2512.

[29] B. O'Regan, M. Gratzel, A low-cost, high-efficiency solar cell based on dye-sensitized colloidal TiO$_2$ films, Nature, 353 (1991) 737-740.

[30] A. Tricoli, A.S. Wallerand, M. Righettoni, Highly porous TiO$_2$ films for dye sensitized solar cells, J. Mater. Chem., 22 (2012) 14254-14261.

[31] J. Chandrasekaran, D. Nithyaprakash, K.B. Ajjan, S. Maruthamuthu, D. Manoharan, S. Kumar, Hybrid solar cell based on blending of organic and inorganic materials-An overview, Renewable Sus. Ener. Rev., 15 (2011) 1228-1238.

[32] D.J. Kim, M.C. Choi, S.S. Park, H. Kim, C.S. Ha, Mesoporous Titania Films Infiltrated with Conjugated Polymers for Photovoltaic Devices, J. Nanoelectron. Optoelectron., 5 (2010) 277-280.

[33] S. Neyshtadt, M. Kalina, G.L. Frey, Self-organized semiconducting polymer-incorporated mesostructured titania for photovoltaic applications, Adv. Mater., 20 (2008) 2541-2546.

[34] K.M. Coakley, M.D. McGehee, Photovoltaic cells made from conjugated polymers infiltrated into mesoporous titania, Appl. Phys. Lett., 83 (2003) 3380-3382.

[35] K.M. Coakley, Y. Liu, C. Goh, M.D. McGehee, Ordered Organic–Inorganic Bulk Heterojunction Photovoltaic Cells, MRS Bull., 30 (2005) 37-40.

[36] S.-S. Kim, J. Jo, C. Chun, J.-C. Hong, D.-Y. Kim, Hybrid solar cells with ordered TiO2 nanostructures and MEH-PPV, J. Photochem. Photobiol. A, 188 (2007) 364-370.

[37] C.J. Brinker, Evaporation-Induced Self-Assembly: Functional Nanostructures Made Easy, MRS Bull., 29 (2004) 631-640.

[38] V.R. Koganti, D. Dunphy, V. Gowrishankar, M.D. McGehee, X. Li, J. Wang, S.E. Rankin, Generalized Coating Route to Silica and Titania Films with Orthogonally Tilted Cylindrical Nanopore Arrays, Nano Lett., 6 (2006) 2567-2570.

[39] Q. Wu, S.E. Rankin, Tuning the wall thickness and pore orientation in mesoporous titania films prepared with low-temperature aging, J Sol-Gel Sci Technol, 60 (2011) 81-90.

[40] S. Das, Q. Wu, R.K. Garlapalli, S. Nagpure, J. Strzalka, Z. Jiang, S.E. Rankin, In-Situ GISAXS Investigation of Pore Orientation Effects on the Thermal Transformation Mechanism in Mesoporous Titania Thin Films, J. Phys. Chem. C, 118 (2013) 968-976.

[41] S. Nagpure, S. Das, R.K. Garlapalli, J. Strzalka, S.E. Rankin, In Situ GISAXS Investigation of Low-Temperature Aging in Oriented Surfactant-Mesostructured Titania Thin Films, J. Phys. Chem. C, 119 (2015) 22970-22984.

[42] S. Das, S. Nagpure, R.K. Garlapalli, Q. Wu, S.Z. Islam, J. Strzalka, S.E. Rankin, Pore orientation effects on the kinetics of mesostructure loss in surfactant templated titania thin films, Phys. Chem. Chem. Phys., 18 (2016) 2896-2905.

[43] J.H. Pan, Z. Lei, W.I. Lee, Z. Xiong, Q. Wang, X.S. Zhao, Mesoporous TiO$_2$ photocatalytic films on stainless steel for water decontamination, Cat. Sci. Technol. , 2 (2012) 147-155.

[44] T. Kimura, N. Miyamoto, X. Meng, T. Ohji, K. Kato, Rapid Fabrication of Mesoporous Titania Films with Controlled Macroporosity to Improve Photocatalytic Property, Chem. Asian J., 4 (2009) 1486-1493.

[45] X. Meng, T. Kimura, T. Ohji, K. Kato, Triblock copolymer templated semi-crystalline mesoporous titania films containing emulsion-induced macropores, J. Mater. Chem., 19 (2009) 1894-1900.

[46] J.H. Pan, W.I. Lee, Preparation of Highly Ordered Cubic Mesoporous WO_3/TiO_2 Films and Their Photocatalytic Properties, Chem. Mater., 18 (2006) 847-853.

[47] E.L. Crepaldi, G.J.D.A.A. Soler-Illia, D. Grosso, F. Cagnol, F. Ribot, C. Sanchez, Controlled Formation of Highly Organized Mesoporous Titania Thin Films: From Mesostructured Hybrids to Mesoporous Nanoanatase TiO_2, J. Am. Chem. Soc., 125 (2003) 9770-9786.

[48] S.Z. Islam, A. Reed, N. Wanninayake, D.Y. Kim, S.E. Rankin, Remarkable Enhancement of Photocatalytic Water Oxidation in N_2/Ar Plasma Treated, Mesoporous TiO_2 Films, J. Phys. Chem. C, 120 (2016) 14069-14081.

[49] S.Z. Islam, A. Reed, D.Y. Kim, S.E. Rankin, N_2/Ar plasma induced doping of ordered mesoporous TiO_2 thin films for visible light active photocatalysis, Micropor. Mesopor. Mater., 220 (2016) 120-128.

[50] S.Z. Islam, S.E. Rankin, Hydrazine-based synergistic Ti(III)/N doping of surfactant-templated TiO_2 thin films for enhanced visible light photocatalysis, Mater. Chem. Phys., 182 (2016) 382-393.

[51] T.A. Kandiel, A.A. Ismail, D.W. Bahnemann, Mesoporous TiO_2 nanostructures: a route to minimize Pt loading on titania photocatalysts for hydrogen production, Phys. Chem. Chem. Phys., 13 (2011) 20155-20161.

[52] A.A. Ismail, T.A. Kandiel, D.W. Bahnemann, Novel (and better?) titania-based photocatalysts: Brookite nanorods and mesoporous structures, J. Photochem. Photobiol. B, 216 (2010) 183-193.

[53] A.A. Ismail, D.W. Bahnemann, L. Robben, V. Yarovyi, M. Wark, Palladium Doped Porous Titania Photocatalysts: Impact of Mesoporous Order and Crystallinity, Chem. Mater., 22 (2009) 108-116.

[54] Q. Yuan, Y. Liu, L.L. Li, Z.X. Li, C.J. Fang, W.T. Duan, X.G. Li, C.H. Yan, Highly ordered mesoporous titania–zirconia photocatalyst for applications in degradation of rhodamine-B and hydrogen evolution, Micropor. Mesopor. Mater., 124 (2009) 169-178.

[55] X. Zhang, J.H. Pan, A.J. Du, J. Ng, D.D. Sun, J.O. Leckie, Fabrication and photocatalytic activity of porous TiO_2 nanowire microspheres by surfactant-mediated spray drying process, MRS Bull., 44 (2009) 1070-1076.

[56] G.M. Veith, L. Baggetto, R.L. Sacci, R.R. Unocic, W.E. Tenhaeff, J.F. Browning, Direct measurement of the chemical reactivity of silicon electrodes with $LiPF_6$-based battery electrolytes, Chem. Comm., 50 (2014) 3081-3084.

[57] P. Feng, X. Bu, D.J. Pine, Control of Pore Sizes in Mesoporous Silica Templated by Liquid Crystals in Block Copolymer−Cosurfactant−Water Systems, Langmuir, 16 (2000) 5304-5310.

[58] M. Manceau, A. Rivaton, J.L. Gardette, S. Guillerez, N. Lemaître, The mechanism of photo- and thermooxidation of poly(3-hexylthiophene) (P3HT) reconsidered, Polym. Degrad. Stab., 94 (2009) 898-907.

[59] P.J. Brown, D.S. Thomas, A. Köhler, J.S. Wilson, J.S. Kim, C.M. Ramsdale, H. Sirringhaus, R.H. Friend, Effect of interchain interactions on the absorption and emission of poly(3-hexylthiophene), Phys. Rev. B, 67 (2003) 064203.

[60] M.H. Kim, M. Suh, V. Gowrishankar, M.D. McGehee, Y.U. Kwon, Confinement Effects of P3HT in Nanochannels and Their Implications for Bulk Heterojunction Solar Cells, J. Nanosci. Nanotechnol., 10 (2010) 279-284.

[61] A. Nelson, Co-refinement of multiple-contrast neutron/X-ray reflectivity data using MOTOFIT, J. Appl. Crystallogr., 39 (2006) 273-276.

[62] M. Rawolle, K. Sarkar, M.A. Niedermeier, M. Schindler, P. Lellig, J.S. Gutmann, J.F. Moulin, M. Haese-Seiller, A.S. Wochnik, C. Scheu, P. Müller-Buschbaum, Infiltration of Polymer Hole-Conductor into Mesoporous Titania Structures for Solid-State Dye-Sensitized Solar Cells, ACS Appl. Mater. Interfaces, 5 (2012) 719-729.

[63] M.G. Harrison, J. Grüner, G.C.W. Spencer, Analysis of the photocurrent action spectra of MEH-PPV polymer photodiodes, Phys. Rev. B, 55 (1997) 7831-7849.

[64] J. Martin, J. Maiz, J. Sacristan, C. Mijangos, Tailored polymer-based nanorods and nanotubes by "template synthesis": From preparation to applications, Polymer, 53 (2012) 1149-1166.

[65] J. Xu, J. Wang, M. Mitchell, P. Mukherjee, M. Jeffries-El, J.W. Petrich, Z. Lin, Organic−Inorganic Nanocomposites via Directly Grafting Conjugated Polymers onto Quantum Dots, J. Am. Chem. Soc., 129 (2007) 12828-12833.

[66] C.Y. Kwong, W.C.H. Choy, A.B. Djurišić, P.C. Chui, K.W. Cheng, W.K. Chan, Poly(3-hexylthiophene):TiO$_2$ nanocomposites for solar cell applications, Nanotechnology, 15 (2004) 1156.

[67] B. Park, Y.H. Huh, M. Kim, Surfactant additives for improved photovoltaic effect of polymer solar cells, J. Mater. Chem., 20 (2010) 10862-10868.

[68] C.S. Lim, S.H. Im, J.A. Chang, Y.H. Lee, H.J. Kim, S.I. Seok, Improvement of external quantum efficiency depressed by visible light-absorbing hole transport material in solid-state semiconductor-sensitized heterojunction solar cells, Nanoscale, 4 (2012) 429-432.

[69] R. Bkakri, O.E. Kusmartseva, F.V. Kusmartsev, M. Song, A. Bouazizi, Degree of phase separation effects on the charge transfer properties of P3HT:Graphene nanocomposites, J. Lumin., 161 (2015) 264-270.

[70] D. Jarzab, F. Cordella, M. Lenes, F.B. Kooistra, P.W.M. Blom, J.C. Hummelen, M.A. Loi, Charge Transfer Dynamics in Polymer−Fullerene Blends for Efficient Solar Cells, J. Phys. Chem. B, 113 (2009) 16513-16517.

[71] M.M. Stylianakis, E. Stratakis, E. Koudoumas, E. Kymakis, S.H. Anastasiadis, Organic Bulk Heterojunction Photovoltaic Devices Based on Polythiophene−Graphene Composites, ACS Appl. Mater. Interfaces, 4 (2012) 4864-4870.
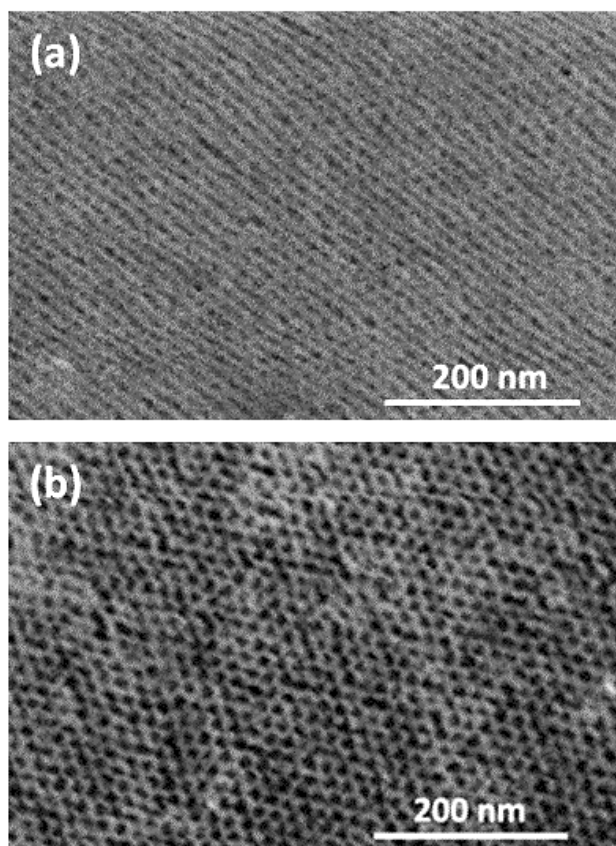
Figure 1. Representative plan view SEM images of mesoporous titania films prepared on (a) plain glass and (b) F127-modified glass prepared from sols containing 1.26 g F127 and 30 g of ethanol, aged at 4 °C and calcined at 400 °C at the rate of 25 °C/min.
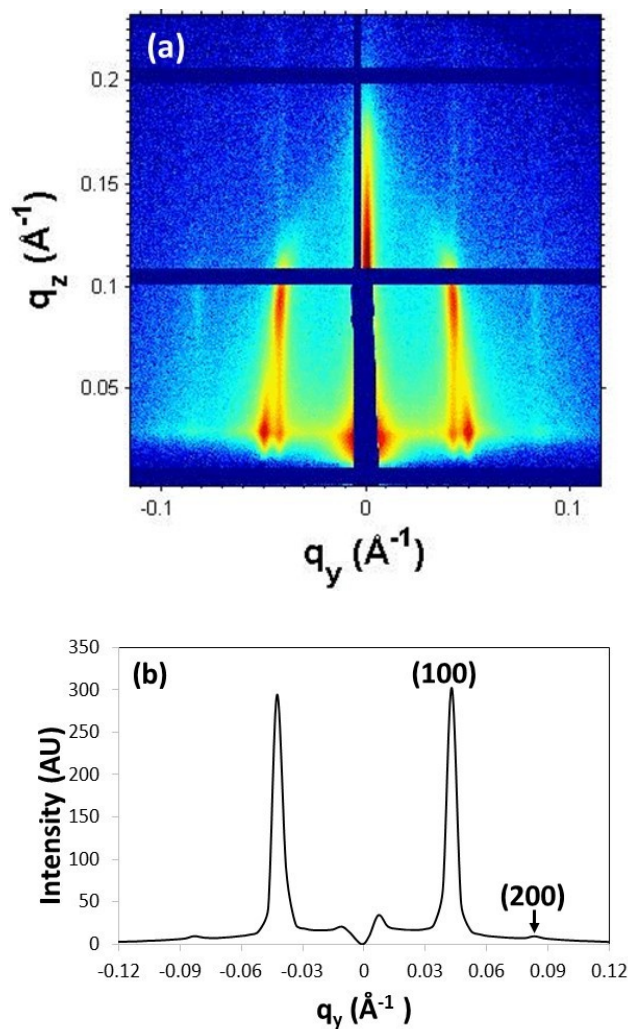
Figure 2. (a) GISAXS pattern of nanoporous titania film prepared on modified glass after calcination at 400° C at a rate of 25 °C/min and (b) the corresponding 1D linecut derived by integrating along the q_z direction from 0.08-0.1 Å^{-1}.
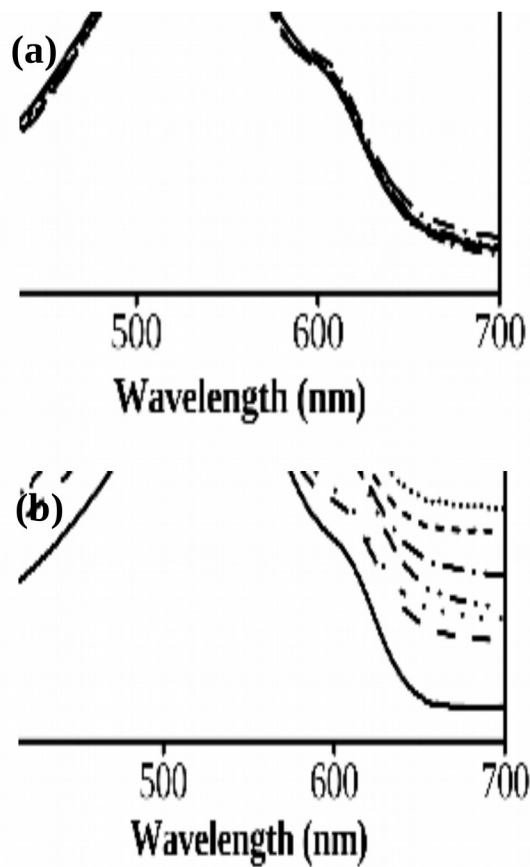
Figure 3. UV-vis absorption spectra of (a) regioregular P3HT and (b) regioregular P3HT infiltrated into titania films with thickness of 120 nm after annealing under vacuum for the indicated times at 200° C (The data has been shifted in part (b) for absorbance values).
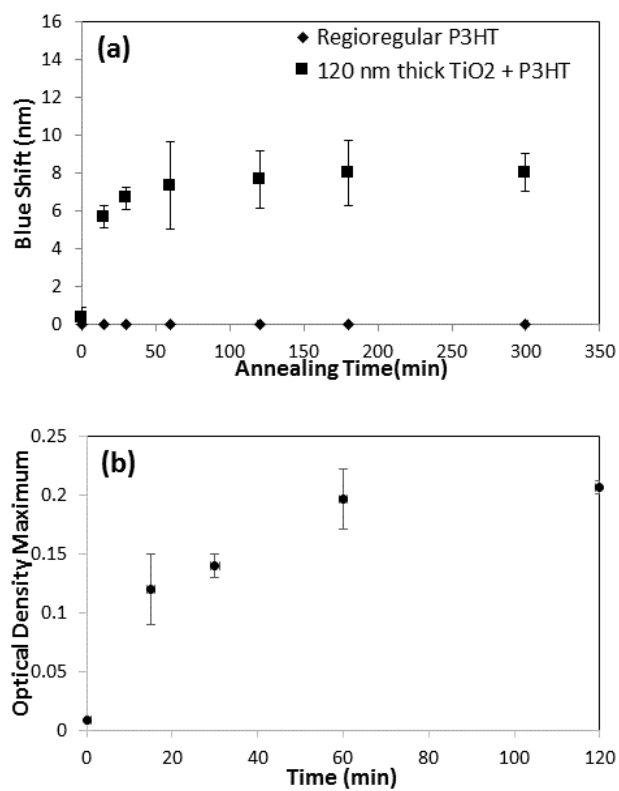
Figure 4. (a) Blue shift of P3HT UV-vis absorbance maximum as a function of annealing time and (b) optical density of embedded P3HT after infiltration for varying periods of time at 200 °C under vacuum.
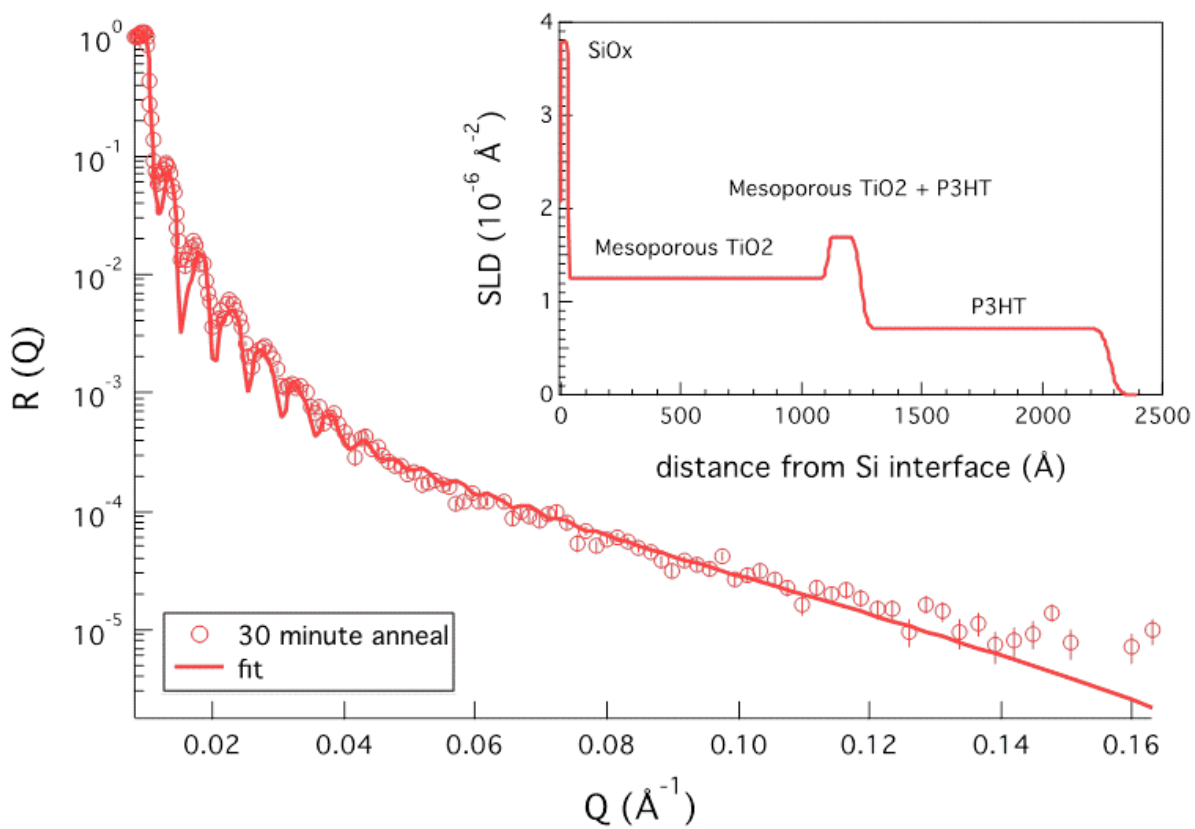
Figure 5. Neutron reflectivity profile of P3HT infiltrated into the nanopores of titania after annealing at 200º C for 30 minutes. The inset shows that scattering length density (SLD) profile of the fitted model.
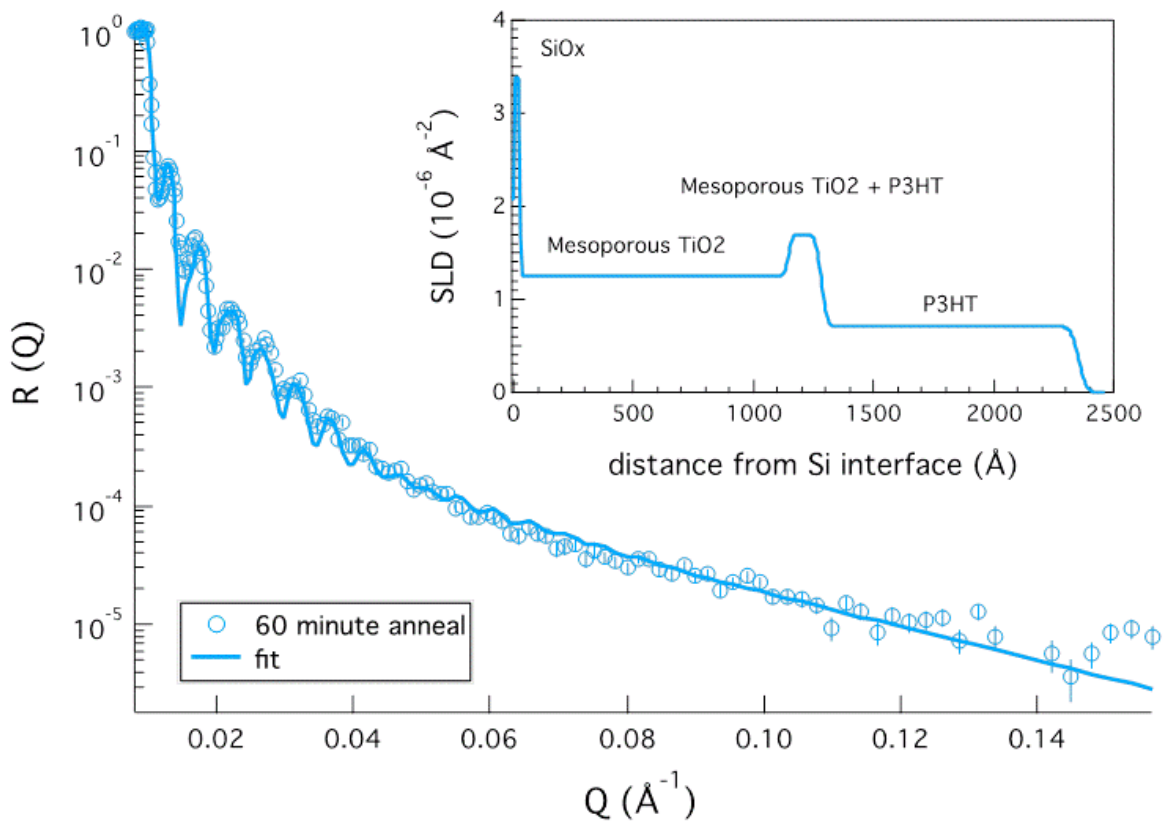
Figure 6. Neutron reflectivity profile of P3HT infiltrated into the nanopores of titania after annealing at 200º C for 60 minutes. The inset shows that scattering length density (SLD) profile of the fitted model.
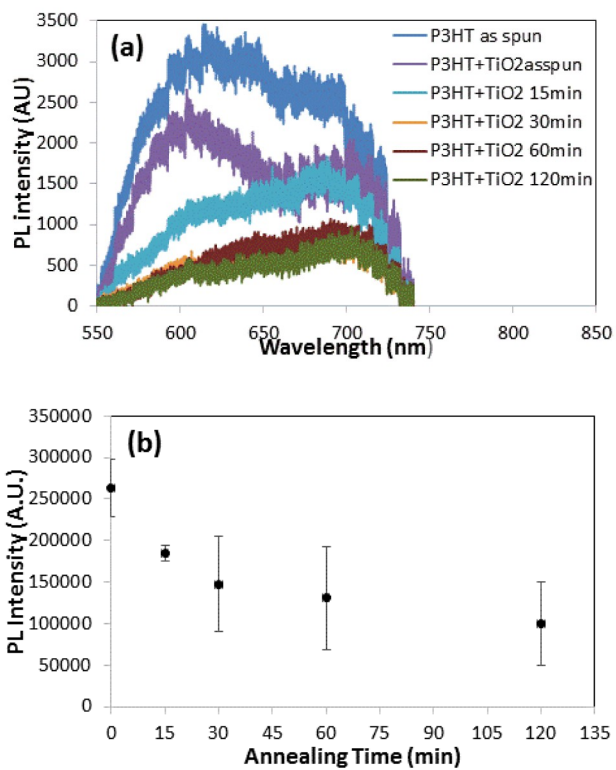
Figure 7. (a).PL spectra for P3HT infiltrated into nanoporous TiO_2 by spin coating 1 wt% P3HT solution followed by annealing at 200 °C for the indicated time and comparison with as spun P3HT, and (b) integrated PL intensity for P3HT infiltrated into nanoporous TiO_2 as a function of annealing time. The error bars represent the standard deviation of the PL intensity of three different samples.

Table 1. Characteristics of layers obtained by fiting a multilayer model to the neutron reflectivity profile of P3HT infiltrated into the nanopores of titania after annealing at 200° C for 30 minutes.

Layer	Thickness (Å)	SLD ($*10^{-6}$ Å^{-2})	Roughness (Å)
P3HT	1035	0.72	27
Interface	139	1.7	19
Mesoporous TiO_2	1078	1.25	11
SiO_x	30	3.78	2

Table 2. Characteristics of layers obtained by fiting a multilayer model to the neutron reflectivity profile of P3HT infiltrated into the nanopores of titania after annealing at 200° C for 60 minutes.

Layer	Thickness (Å)	SLD ($*10^{-6}$ Å^{-2})	Roughness (Å)
P3HT	1072	0.7	26
Interface	137	1.7	19
Mesoporous TiO_2	1118	1.25	14
SiO_x	27	3.4	3

Graphical Abstract